Int. J. Heat Mass Transfer. Vol. 15, pp. 315–326. Pergamon Press 1972. Printed in Great Britain

EFFECTS OF NONCONDENSABLE GAS AND FORCED FLOW ON LAMINAR FILM CONDENSATION*

V. E. DENNY and V. J. JUSIONIS
University of California, Los Angeles, California 90024, U.S.A.

(*Received* 13 *April* 1971)

Abstract—An analytical study of the effects of noncondensable gas and forced flow on laminar film condensation is presented. Due to the markedly nonsimilar character of the coupled two phase flow problem, the governing conservation equations in the vapor phase were solved numerically by means of a forward marching technique. Interfacial boundary conditions at each step were extracted from a locally valid Nusselt-type analysis of the falling film. Locally variable properties in the liquid were evaluated by means of the reference temperature concept, while those in the vapor were calculated according to kinetic theory.

Heat-transfer results, in the form q/q_{Nu} vs. x, are reported for six vapors—water, ammonia, Freon-12, ethanol, butanol, and carbon tetrachloride—condensing on a vertical surface at 80°F. Results were obtained for vapor velocities of 1·0 and 10·0 ft/s, saturation temperatures of 90, 100 and 120°F, and mass fraction air of 0·001 and 0·01. Guided by the numerical data, a semi-empirical calculation method is developed which provides a satisfactory basis for engineering calculations.

NOMENCLATURE

$\mathscr{B}$, mass-transfer driving force;
C_p, heat capacity;
$\mathscr{D}_{12}$, binary diffusion coefficient;
g, standard acceleration of gravity;
$\mathscr{g}$, mass-transfer conductance;
k, thermal conductivity;
m, mass fraction;
$\dot{m}$, condensation rate per unit area $= (\rho v)|_{v,i}$;
M, molecular weight;
p, partial pressure;
P, total pressure;
Pr, Prandtl number $= \mu C_p/k$;
q, wall heat flux;
q_{Nu}, Nusselt heat flux $= [k^3(T_e - T_w)^3 \rho g \lambda/4xv]^{\frac{1}{4}}$;
R, specific gas constant $= \mathscr{R}/M$;
$\mathscr{R}$, universal gas constant;
Re_x, Reynolds number $= u_e x/v_e$;
Sc, Schmidt number $= v/\mathscr{D}_{12}$;
T, absolute temperature;
u, v, velocity components;
x, mole fraction;
x, y, boundary-layer coordinates.

Greek symbols

α, parameter for defining the reference temperature;
δ, condensate film thickness;
η, suction parameter $= -\dot{m}Re_x^{\frac{1}{2}}/\rho_{v,e}u_e$;
λ, latent heat of vaporization;
μ, absolute viscosity;
ν, kinematic viscosity;
ρ, density;
τ, shear stress.

Subscripts

e, at the vapor boundary-layer edge;
i, at the interface;
l, in the liquid phase;
r, at the reference state;
v, in the vapor phase;
w, at the wall;
x, at position x;
1, of the condensing species;
2, of air.

INTRODUCTION

IN A RECENT paper [1], the authors investigated

* This work was supported in part by the State of California through the University of California Statewide Water Resources Center on Grant No. 4-442595-20539. Computer time for the numerical computations was provided by the Campus Computing Network of the University of California, Los Angeles.

laminar film condensation for steam–air mixtures undergoing forced flow down a vertical surface. Numerical solutions of the resulting nonsimilar problem were reported for vapor velocities and mass fractions air in the ranges 0·1–10·0 ft/s and 0·001–0·1, respectively. The vapor mixture was saturated, the saturation pressure being for the most part one atmosphere. The nonsimilar character of the results was particularly evident near the leading edge of the vertical surface, where the ratio of the actual heat flux, q, to the classical Nusselt result based on overall temperature drop, q_{Nu}, decreased very rapidly with increasing distance x down the surface. Under conditions of reduced vapor velocity and/or elevated mass fraction air, q/q_{Nu} approached asymptotically the similar solutions of Minkowycz and Sparrow [2], wherein the free stream is stationary. However, at vapor velocities approaching 10 ft/s, forced flow had a sustained and marked effect on q/q_{Nu}, the nonsimilar results remaining much higher than the corresponding similar solutions in the interval $0 < x < 0{\cdot}5$ ft.

Since most industrial applications are characterized by forced convection in the vapor phase, additional study of the forced flow situation is warranted. Furthermore, with the exception of the constant property analysis of Sparrow and Lin [3], again in the absence of forced flow, little analytical attention has been directed towards vapor mixtures other than water vapor–air. The objectives of this paper are two-fold. First, the effects of forced flow are investigated for steam–air mixtures in the low pressure regime and for mixtures of selected organic vapors and air at normal condenser temperatures. Numerical solutions of the governing conservation equations are obtained using the methods discussed in [1]. Second, a semi-empirical predictive theory is developed which provides a more convenient basis for engineering calculations.

A schematic diagram of the physical situation involved is shown in Fig. 1. The vertical condenser surface is at a uniform temperature T_w. The

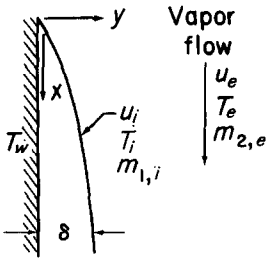

FIG. 1. Schematic of physical situation.

coordinates along and normal to the surface are x and y, respectively, and the corresponding velocity components are u and v. At some distance from the surface the vapor mixture has velocity u_e, temperature T_e, and noncondensable gas concentration $m_{2,e}$. The system pressure P_e is determined from T_e and $m_{2,e}$, assuming the free stream is saturated. The condensate film has thickness δ, which varies with x. At the vapor–liquid interface, the temperature T_i and, hence, the mass fraction $m_{1,i}$ are unknown and must be determined in the course of the analysis. With forced flow, T_i and $m_{1,i}$ are of course functions of x.

ANALYSIS

Governing equations and boundary conditions

For the vapor phase, the equations governing conservation of mass, momentum, species, and energy are, respectively,

$$\frac{\partial}{\partial x}(\rho_v u) + \frac{\partial}{\partial y}(\rho_v v) = 0 \tag{1}$$

$$\rho_v u \frac{\partial u}{\partial x} + \rho_v v \frac{\partial u}{\partial y} = \frac{\partial}{\partial y}\left(\mu_v \frac{\partial u}{\partial y}\right) + g(\rho_v - \rho_{v,e}) \tag{2}$$

$$\rho_v u \frac{\partial m_1}{\partial x} + \rho_v v \frac{\partial m_1}{\partial y} = \frac{\partial}{\partial y}\left(\rho_v \mathscr{D}_{12} \frac{\partial m_1}{\partial y}\right) \tag{3}$$

$$\rho_v u \frac{\partial T}{\partial x} + \rho_v v \frac{\partial T}{\partial y} = \frac{\partial}{\partial y}\left(\frac{k}{C_{p,v}} \frac{\partial T}{\partial y}\right) + \frac{k_v}{C_{p,v}} \frac{\partial T}{\partial y} \frac{\partial \ln C_{p,v}}{\partial y} + \frac{\rho_v \mathscr{D}_{12}}{C_{p,v}} (C_{p,1} - C_{p,2}) \frac{\partial m_1}{\partial y} \frac{\partial T}{\partial y}. \tag{4}$$

Since low velocity flow is being considered, viscous dissipation and compressibility effects are omitted in equation (4). In addition, thermal diffusion and diffusion-thermo (Dufour effect) are ignored in view of results obtained by Minkowycz [4].

For the liquid phase, the physical properties ρ, μ, and k were evaluated at the reference temperature $T_r(x) = T_w + \alpha(T_i - T_w)$, with values of α being taken from [5]. Invoking the Nusselt assumptions yields

$$0 = \mu_l \frac{d^2u}{dy^2} + g(\rho_l - \rho_{v,e}) \tag{5}$$

$$0 = \frac{d^2T}{dy^2}. \tag{6}$$

Equations (1)–(6) are subject to the boundary conditions

$$u \to u_e, \quad m_1 \to m_{1,e}, \quad T \to T_e \tag{7}$$

as $y \to \infty$;

$$u = 0, \quad T = T_w \tag{8}$$

at $y = 0$; and

$$u|_{l,i} = u|_{v,i} = u_i \tag{9}$$

$$T|_{l,i} = T|_{v,i} = T_i \tag{10}$$

$$\mu \left.\frac{\partial u}{\partial y}\right|_{l,i} = \mu \left.\frac{\partial u}{\partial y}\right|_{v,i} = -\tau_i \tag{11}$$

$$\frac{d}{dx}\int_0^\delta \rho u \, dy\Big|_l = -\dot{m} = \frac{\rho \mathscr{D}_{12}}{1 - m_1} \left.\frac{\partial m_1}{\partial y}\right|_{v,i} \tag{12}$$

$$k \left.\frac{\partial T}{\partial y}\right|_{l,i} = -\dot{m}\lambda + k \left.\frac{\partial T}{\partial y}\right|_{v,i} \tag{13}$$

at $y = \delta(x)$.

In addition, there is required an equation of state and a thermodynamic constraint at the interface. Assuming ideal gas behavior prevails at the low pressures under consideration and that the interface is at equilibrium [4, 6], there obtains

$$P_e = \rho_v RT, \quad T_i = T_i(m_{1,i}, P_e). \tag{14}$$

Closure of the overall problem is effected by means of an energy balance on the liquid film, which serves to extract the film thickness δ:

$$\int_0^x k \frac{\partial T}{\partial y} dx\Big|_{y=0} = \int_0^\delta \rho u[\lambda + C_p(T_i - T)] dy\Big|_x - \int_0^x k \frac{\partial T}{\partial y} dx\Big|_{v,i}. \tag{15}$$

Following Patankar and Spalding [7], equations (1)–(4) were solved by means of finite difference methods, iteration being required at each marching step to achieve compatibility with the liquid side problem. A detailed description of the overall numerical procedure is given in [1]. As introduction to the next section, it is noted that an approximate solution of the problem could be effected provided $T_i(x)$ were known; for, in such an event the liquid side problem, apart from the second order effects of vapor drag and vapor-side heat conduction, is decoupled from the vapor-side problem.

An approximate calculation method

Although $T_i(x)$ is *a priori* unknown, $T_i(0) \simeq T_e$ as shown in [1]. Furthermore, $T_i(x)$ decreases monotonically with increasing x (which behavior is in apposition to that for the similar problem, for which T_i is constant). Thus, the liquid side problem may be viewed as a non-isothermal "wall" problem, $T_i(x)$ assuming the role of T_w in the analysis presented in [5]. As in [5], equations (5), (6), (8), (10), (11), (13) and (15) are solved subject to the approximation [8]

$$\tau_i = \dot{m}(u_e - u_i)$$

and neglecting vapor-side heat conduction. If it further is assumed that $Pr_l\lambda/C_{p,i}(T_i - T_w) \gg 1$ and physical property variations in the x-direction are negligible there obtains directly from [5]

$$q(x) = k_l \Delta T \left[\frac{f_1}{v_l x} \frac{u_e + (u_e^2 + 16g^* x f_2/r)^{\frac{1}{2}}}{8}\right]^{\frac{1}{2}} \tag{16}$$

where

$$g^* = g(1 - \rho_{v,e}/\rho_l)$$

$$r = 1/[(Pr_l)(\lambda/C_{p,l}\,\Delta T) + 0{\cdot}354] \doteq k_l\,\Delta T/\mu_l\lambda$$

$$f_1 \doteq 2\Delta T/\tilde{\Delta T} - 1$$

$$f_2 \doteq (\tilde{\Delta T}/\Delta T)/(2 - \tilde{\Delta T}/\Delta T)^2$$

and

$$\Delta T = T_i(x) - T_w, \quad \tilde{\Delta T} = \int_0^x \Delta T \mathrm{d}x/x.$$

However, for $\Delta T < \tilde{\Delta T}/2$, $f_1 < 0$ and equation (16) becomes singular. Fortunately, for ΔT decreasing with increasing x the effects of variable ΔT are modest (see Table 3, [5]) and, to excellent approximation, equation (16) may be written

$$q(x) = \frac{k_l\,\Delta T}{F(\theta)}\left[\frac{u_e + (u_e^2 + 16g^*xk_l\,\Delta T/\mu_l\lambda)^{\frac{1}{2}}}{8\nu_l x}\right]^{\frac{1}{2}} \tag{17}$$

where $F(\theta)$ represents a best fit to the nonisothermal wall results of [5]:

$$F(\theta) = 1 + 0{\cdot}046\theta + 0{\cdot}069\theta^2,$$

$$\theta = (T_e - T_i)/(T_e - T_w).$$

Alternatively, equation (17) may be written in terms of equation (12) as

$$q(x) \doteq -\dot{m}\lambda = -g\mathscr{B}\lambda \tag{18}$$

where, after Spalding [9], the mass-transfer conductance g is just

$$g = \frac{\rho\mathscr{D}_{12}}{m_{1,e} - m_1}\left.\frac{\partial m_1}{\partial y}\right|_{v,i} \tag{19}$$

while the driving force $\mathscr{B}$ is defined as

$$\mathscr{B} = (m_{1,e} - m_{1,i})/(m_{1,i} - 1) = m_{2,e}/m_{2,i} - 1. \tag{20}$$

Since $m_{1,i} = m_{1,i}(T_i, P_e)$, equations (17)–(20) constitute essentially two equations in q and T_i, providing a working expression for the conductance g can be established. A promising approach in the latter context is to adjust an appropriate similarity result, say that of Acrivos [10],

$$g = \rho_{v,e}u_eSc_e^{-1}Re_x^{-\frac{1}{2}}/[2(1 + \mathscr{B})(1 + Sc_e^{-1})]^{\frac{1}{2}} \tag{21}$$

so as to accommodate nonsimilar effects. Further elaboration on this point is deferred to the discussion.

Thermophysical properties

The properties ρ_l, $c_{p,l}$, k_l, u_l and λ were extracted from sources listed in [5] and evaluated by means of least-squares analysis at either T_r or, in the case of λ, at T_i. For the steam–air mixtures, procedures recommended by Minkowycz [4] were followed. Briefly, mixture rules

Table 1. Thermophysical property data and references†*

Species	σ (Å)	ε/k (°K)	C_p	$p_1\|_{v,i}$
Air	3·689 [14]	84·0 [14]	[12]	—
Ammonia	3·15 [11]	358·0 [11]	[18]	[21]
Freon-12	5·11 [15]	288·0 [15]	[18]	[21]
Carbon tetrachloride	5·973 [16]	315·0 [16]	[19]	[21]
Ethyl alcohol	4·455 [16]	391·0 [16]	[20]	[22]
n-Butyl alcohol	6·00 [17]	263·0 [17]	[14]	[23]
Water	—	—	[13]	[13]

* For steam–air, $\sigma_{12} = 3{\cdot}724$ Å and $\varepsilon_{12}/k = 50$°K [4]; otherwise,

$$\sigma_{12} = (\sigma_1 + \sigma_2)/2, \quad \varepsilon_{12}/k = [(\varepsilon_1/k)(\varepsilon_2/k)]^{\frac{1}{2}}.$$

† $\Omega^{(l,s)^*}$ from Table I–M, [14].

as set forth by Mason and Monchik [11] were used to calculate, first, $\mathscr{D}_{12}$ and then μ_v and k_v, assuming a Lennard–Jones interaction potential. Pure species values for μ and k were taken from [12]. C_p of air was taken from [12] while that for steam was taken from [13]. For the organic vapor–air mixtures, the procedures differed slightly in that pure species values of μ and k were calculated according to kinetic theory [14]. Pertinent sources of information for the gas phase property calculations and for vapor pressure data are listed in Table 1.

RESULTS AND DISCUSSION

Accuracy of the numerical data

The principal sources of error in the numerical data are truncation errors in the finite difference analogues of the cross-stream derivatives. Although these errors could in principle be rendered negligibly small by using a sufficiently large number of node-points across the boundary layer, the cost for doing so is prohibitive. For this study, 100 points were used and, on the basis of numerical experiments using fewer node-points, it is estimated that the results are in error by at most a few per cent, the largest errors occurring under conditions for which $\rho_{v,e}$ is very small. (For difficult cases, a typical run required about 300 seconds of machine time on an IBM 360/91 computer and cost about $150.) Additional comments on the accuracy of the numerical method appear in [1].

Correlation of the mass transfer conductance

In applying equations (17) and (18), an expression for g is required. For condensation processes in the presence of noncondensable gas, the mass transfer driving force $\mathscr{B}$ tends towards -1. Thus, an appropriate starting point for predicting g is the similarity result of Acrivos, equation (21), which after isolating $Re_x^{-\frac{1}{2}}$ on the right hand side yields a straight line with slope $-\frac{1}{2}$ on a log–log plot as shown in Fig. 2. Actual values of the ordinate,

$$g[2(1+\mathscr{B})(1+Sc_e^{-1})]^{\frac{1}{2}}/\rho_{v,e}u_eSc_e^{-1},$$

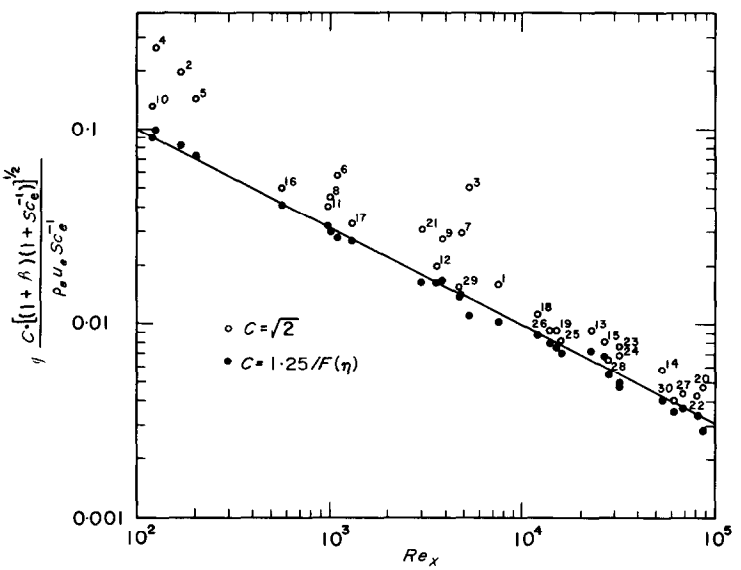

FIG. 2. Correlation of mass transfer conductance.

Table 2. Case history data for Fig. 2.

Case	Fluid	T_e (°F)	u_e (ft/s)	$m_{2,e}$	$\rho_{v,e}$ (lb/ft^3)	Sc_e^{-1}	x (ft)	η	$m_{2,e}/m_{2,w}$
1	CCl_4	100	1	0·01	0·1010	4·46	0·529	9·40	0·0860
2	C_4H_9OH	120	1	0·01	0·0075	3·25	0·122	15·83	0·0180
3	CCl_4	120	1	0·001	0·1000	4·71	0·253	10·76	0·0045
4	C_4H_9OH	90	1	0·001	0·0028	3·39	0·227	10·97	0·0066
5	C_4H_9OH	100	1	0·01	0·0039	3·27	0·269	15·74	0·0324
6	C_2H_5OH	120	1	0·001	0·0292	2·55	0·233	8·04	0·0017
7	CCl_4	120	1	0·01	0·1504	4·42	0·233	10·61	0·0428
8	C_2H_5OH	120	1	0·01	0·0295	2·51	0·216	7·31	0·0169
9	C_4H_9OH	120	10	0·01	0·0075	3·25	0·278	6·24	0·0180
10	C_4H_9OH	90	1	0·01	0·0028	3·29	0·220	10·60	0·0620
11	H_2O	100	10	0·01	0·0029	1·78	0·238	6·85	0·0170
12	H_2O	150*	10	0·01	0·0108	1·85	0·254	4·29	0·0191
13	NH_3	120	1	0·001	0·789	1·54	0·222	3·12	0·0017
14	CCl_4	120	10	0·01	0·1504	4·42	0·259	3.42	0·0428
15	NH_3	120	1	0·01	0·797	1.54	0·269	3·13	0·0165
16	C_2H_5OH	90	1	0·01	0·0131	2·53	0·260	4·26	0·0509
17	C_4H_9OH	90	10	0·01	0·0028	3·29	0·238	3·46	0·0618
18	C_2H_5OH	120	10	0·01	0·0295	2·51	0·262	2·55	0·0169
19	CCl_4	100	10	0·01	0·1010	4·46	0·255	2·39	0·0956
20	CCl_2F_2	120	1	0·001	3·32	3·67	0·239	2·47	0·0067
21	CCl_4	90	1	0·01	0·0815	4·48	0·256	5·17	0·1637
22	CCl_2F_2	120	1	0·01	3·35	3·52	0·224	2·39	0·0623
23	CCl_4	100	10	0·001	0·1000	4·74	0·112	2·01	0·0086
24	CCl_4	90	10	0·001	0·1000	4·75	0·266	1·66	0·0197
25	NH_3	90	1	0·001	0·520	1·56	0·225	1·42	0·0042
26	NH_3	90	1	0·01	0·524	1·55	0·250	1·43	0·0418
27	CCl_2F_2	100	1	0·01	2·67	3·54	0·217	1·58	0·1187
28	CCl_4	90	10	0·01	0·0815	4·48	0·251	1·62	0·1637
29	C_2H_5OH	90	10	0·01	0·0131	2·53	0·220	1·32	0·0509
30	CCl_2F_2	90	1	0·01	2·37	3·55	0·234	1·02	0·2140

* $T_w = 130$°F.

as extracted from numerical solutions of the cases listed in Table 2, appear as open circles in the figure. For the markedly nonsimilar problem under investigation here, the agreement, as might be expected, is poor. Although some improvement would obtain on adjusting the slope and intercept of the solid curve, the scatter would still be excessive. Furthermore, little progress acrues on altering the functional dependence of g on $\mathscr{B}$ and Sc_e or on incorporating the effects of variable physical properties. After considerable study, it was concluded that additional parameters are required. Two possibilities are listed in Table 2—the suction parameter [8]

$$\eta = -\dot{m}_{Nu} Re_x^{\frac{1}{2}}/\rho_{v,e} u_e,$$

where $\dot{m}_{Nu} = -q_{Nu}/\lambda$, and an overall "resistance", $m_{2,e}/m_{2,w}$, where $m_{2,w}$ is the mass fraction air which would obtain at the interface provided $T_i = T_w$. As may be seen upon comparing cases in Table 1 with the results in Fig. 2, the deviations between actual values of the ordinate and the $Re_x^{-\frac{1}{2}}$ curve increase, somewhat irregularly, directly with η and inversely with $m_{2,e}/m_{2,w}$. Therefore, equation (21) was modified to give

$$g = 0{\cdot}8\rho_{v,e} u_e Sc_e^{-1} Re_x^{-\frac{1}{2}} F(\eta)/[1 + \mathscr{B})(1 + Sc_e^{-1})]^{\frac{1}{2}} \tag{22}$$

where

$$F(\eta) = 1 + \frac{0{\cdot}0785(M_1/M_2)\eta}{1 + 100 m_{2,e}/m_{2,w}}, \tag{23}$$

the molecular weight ratio M_1/M_2 being required to obtain some degree of universality in the expression for $\mathscr{g}$. Although the results using equation (22) still scatter to some extent (solid circles in Fig. 2), they nonetheless are encouraging. It remains to demonstrate that the proposed expression is generally applicable.

Heat-transfer results

Heat-transfer results, in the form q/q_{Nu} vs. x, are presented in Figs. 3–10. (The solid curves represent the full numerical solutions while the dashed curves represent equations (17) and (18) using equation (22) to predict $\mathscr{g}$.) For the conditions in Fig. 3, the effects of noncondensable gas are seen to be negligible ($\Delta T \simeq T_e - T_w$) and the results serve to validate the use of the asymptotic expression for vapor drag, $\dot{m}(u_e - u_i)$, in deriving equation (16). Only near $x = 0$, where $\eta \ll 2$ [5], is the asymptotic expression seen to be inadequate, the predictions for NH_3 and CCl_2F_2 falling below the numerical solutions as $x \to 0$ due to additional drag (over and above that predicted by the asymptotic results), with its $x^{-\frac{1}{2}}$ dependence for a zero-pressure gradient flow, which has been neglected in equation (16).

In Fig. 4, the effects of noncondensable gas begin to appear. The major trends in the figure, which are evident throughout, are most easily explained in terms of equation (21), referring to Table 2 for appropriate physical property information. For a given $\mathscr{B}$ one would expect, since $\mathscr{g} \alpha (\rho_{v,e} Sc_e^{-1})^{\frac{1}{2}}$ and $q \alpha \dot{m} = \mathscr{g}\mathscr{B}$, that the curves for the individual species would rank as follows: CCl_2F_2, NH_3, CCl_4, C_2H_5OH, C_4H_9OH and H_2O. Thus, CCl_2F_2 and CCl_4 appear to be anomalous. However, for a given

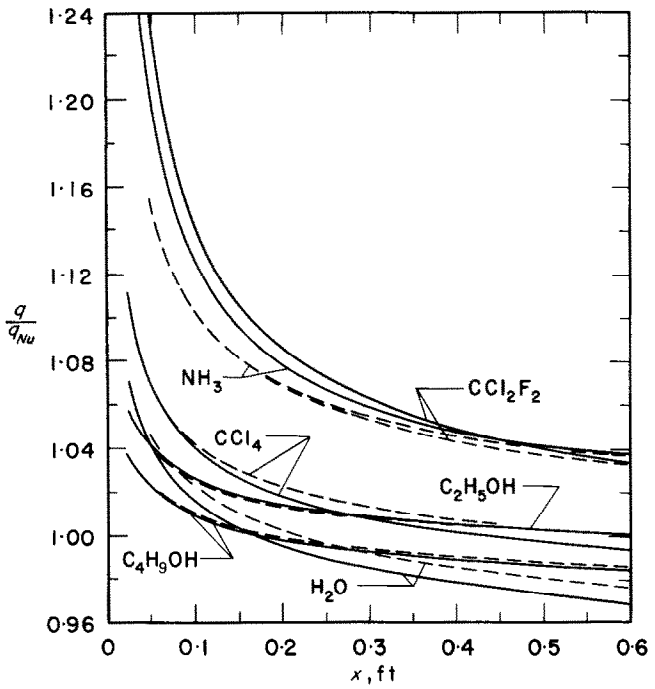

FIG. 3. Condensation heat transfer: $u_e = 10$ ft/s, $T_e = 100°F$, $T_w = 80°F$, $m_{2,e} = 0{\cdot}001$.

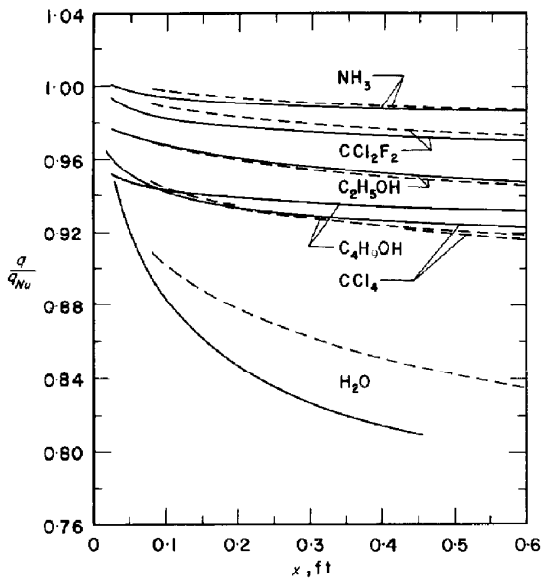

FIG. 4. Condensation heat transfer: $u_e = 1$ ft/s, $T_e = 90°F$, $T_w = 80°F$, $m_{2,e} = 0{\cdot}001$.

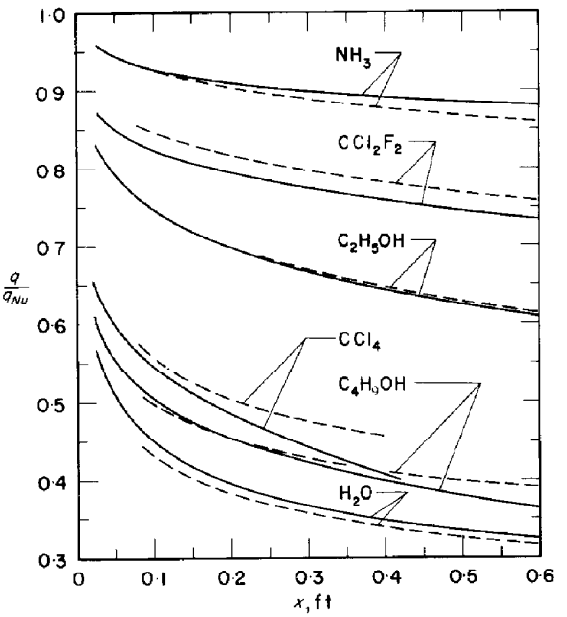

FIG. 5. Condensation heat transfer: $u_e = 1$ ft/s, $T_e = 90°F$, $T_w = 80°F$, $m_{2,e} = 0{\cdot}01$.

$$\mathscr{B} = m_{2,e}/m_{2,i} - 1,$$

that is, for a given $m_{2,i}$, it is readily seen that $\Delta T = T_i - T_w$ is reduced as the molecular weight M_1 of the condensing species increases since

$$x_{2,i} = \frac{P_e - p_{1,i}(T_i)}{P_e} = \frac{m_{2,i}}{m_{2,i} + (M_2/M_1)(1 - m_{2,i})}$$

approaches 1 as M_1 becomes large. (It is this "penalty" which has been incorporated in equation (23) to reduce the effectiveness of η in augmenting the Acrivos result for g.)

The effects of u_e and $T_e - T_w$ are displayed in Figs. 5–10 with $m_{2,e} = 0{\cdot}01$. Since $g \alpha u_e^{\frac{1}{2}}$, interpretation of the effects of increasing u_e are straightforward (compare Figs. 5–7 with 8–10). However, the influence of increasing $T_e - T_w$ (increasing T_e since T_w is fixed) is more subtle. As T_e increases, $\rho_{v,e}$ increases and, hence, so does g. But, $\dot{m}$ also increases, resulting in an enhanced convective inflow of gas which must

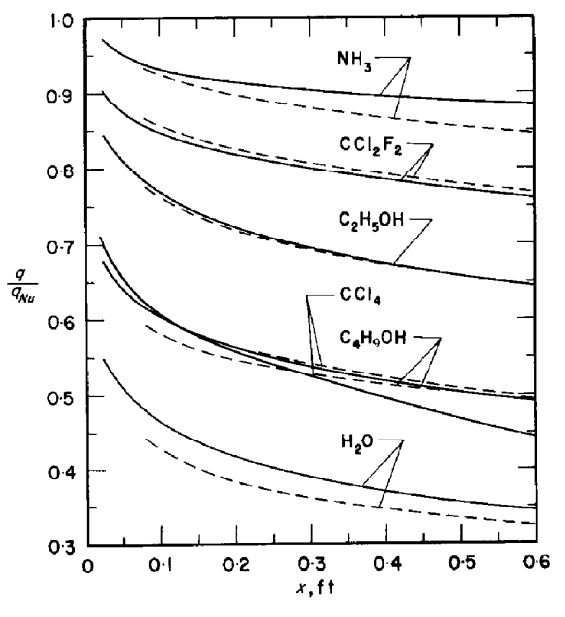

FIG. 6. Condensation heat transfer: $u_e = 1$ ft/s, $T_e = 100°F$, $T_w = 80°F$, $m_{2,e} = 0{\cdot}01$.

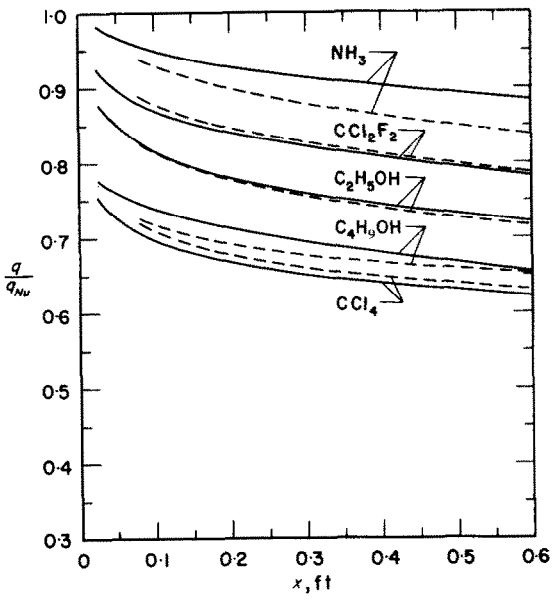

FIG. 7. Condensation heat transfer: $u_e = 1$ ft/s, $T_e = 120°F$, $T_w = 80°F$, $m_{2,e} = 0{\cdot}01$.

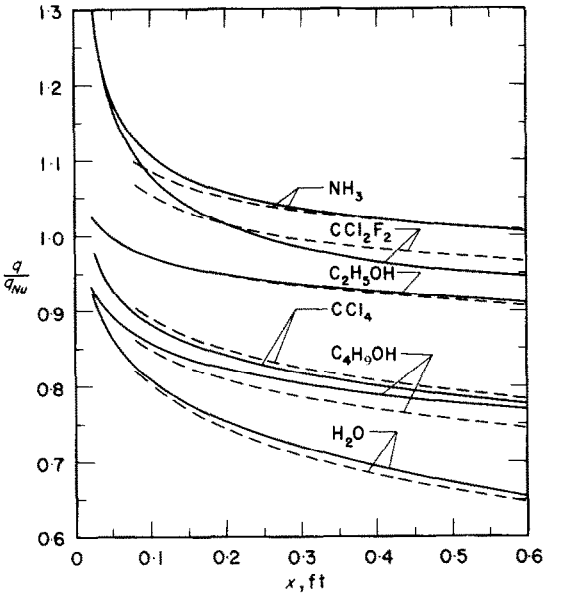

FIG. 9. Condensation heat transfer: $u_e = 10$ ft/s, $T_e = 100°F$, $T_w = 80°F$, $m_{2,e} = 0{\cdot}01$.

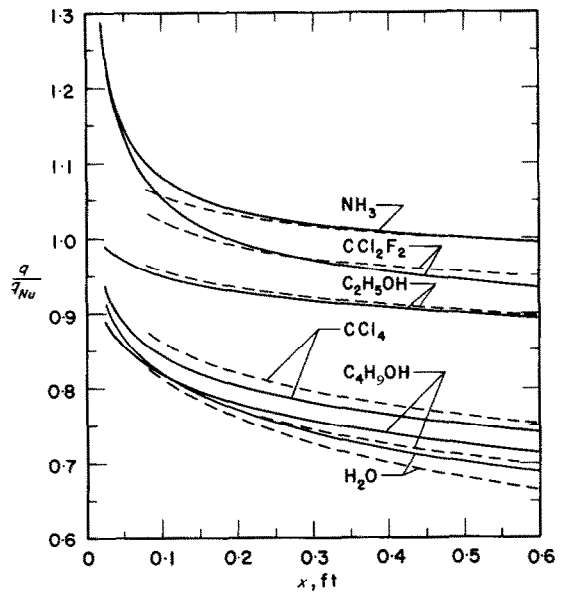

FIG. 8. Condensation heat transfer: $u_e = 10$ ft/s, $T_e = 90°F$, $T_w = 80°F$, $m_{2,e} = 0{\cdot}01$.

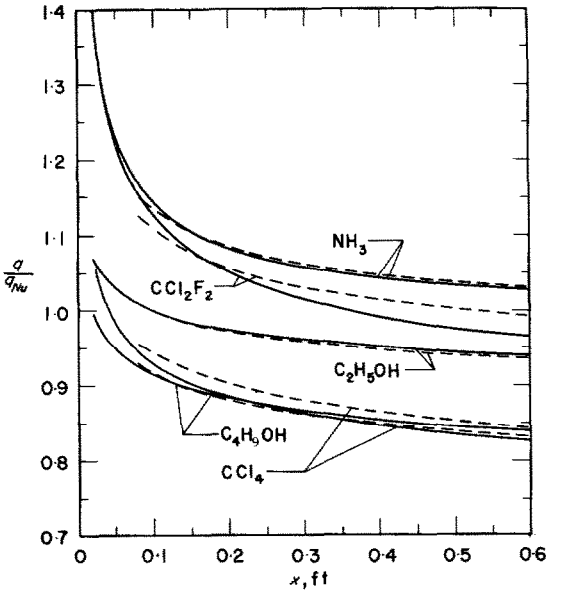

FIG. 10. Condensation heat transfer: $u_e = 10$ ft/s, $T_e = 120°F$, $T_w = 80°F$, $m_{2,e} = 0{\cdot}01$.

be balanced by a diffusive outflow. Depending on the particular situation, then, T_i, that is, q/q_{Nu} may either increase or decrease with increasing T_e.

Considering the complexity of the nonsimilar problem under consideration, the efficacy of equations (17), (18) and (22) in predicting the numerical results is rather remarkable. Only in the case of CCl_4 at reduced vapor velocity and modest suction (Figs. 5 and 6) does the method begin to break down (the discrepancies for H_2O in Figs. 5 and 6 are less serious than they appear because, as discussed earlier, the numerical data is a few per cent high). However, this is due to neglect of the adverse effects of buoyancy on the convective situation, as illustrated in Fig. 11. At $u_e = 1$ ft/s and $T_e = 90°F$

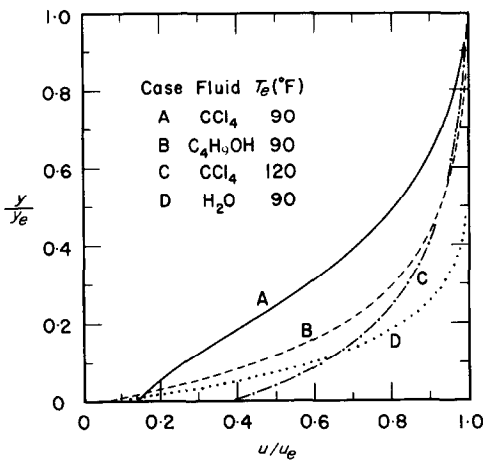

FIG. 11. Effects of buoyancy on velocity profiles: $u_e = 1$ ft/s, $T_w = 80°F$, $m_{2,e} = 0{\cdot}01$, $x \doteq 0{\cdot}4$ ft.

studied, the effects of buoyancy are less pronounced (curves B and D). Apparently, the effects of buoyancy on the velocity field involve a complex interaction between Gr_x/Re_x^2 and, perhaps, suction parameter η. Although attempts to incorporate the effects of mixed free and forced convection met with some success, the limited data available does not warrant their inclusion here.

Further support for the proposed method is displayed in Fig. 12, where some results at

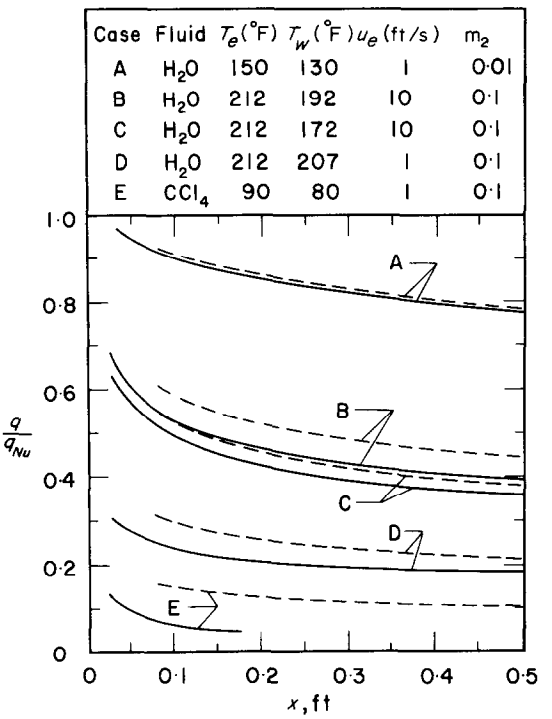

FIG. 12. Condensation heat transfer (numerical solutions for curves A–D from [1]).

(curve A), accumulation of [lighter] air at the interface is having a marked and deleterious effect on the [weak] forced convection situation. However, at $T_e = 120°F$ the velocity profile (curve C) is characteristic of boundary layer flow undergoing strong suction, despite the fact that the ratio of Grashoff number over Reynolds number squared, Gr_x/Re_x^2, is greater in case C than in case A. For other fluids much higher gas concentrations appear. [With the exception of curve A, none of the results in the figure was used to develop equation (22).] Not unexpectedly, the discrepancies between prediction and the presumably exact numerical solutions are larger, particularly near $q/q_{Nu} = 0$; however, they are not catastrophic and the proposed method is seen to provide a satisfactory basis for engineering calculations.

Table 3. Verification of equation (17)

Fluid	T_e (°F)	T_w (°F)	u_e (ft/s)	$m_{2.e}$	x (ft)	T_i (°F)	q/q_{Nu}	q/q_{Nu}*
CCl_4	90	80	1	0·01	0·1	84·70	0·545	0·546
					0·4	83·28	0·403	0·409
C_4H_9OH	90	80	1	0·01	0·1	84·25	0·503	0·502
					0·4	83·17	0·398	0·397
CCl_2F_2	90	80	1	0·01	0·1	87·78	0·824	0·822
					0·4	87·08	0·760	0·760
H_2O	212	192	10	0·1	0·1	200·44	0·525	0·523
					0·4	198·44	0·411	0·411
H_2O	212	172	10	0·1	0·1	187·47	0·488	0·495
					0·4	183·44	0·371	0·376
H_2O	212	207	1	0·1	0·1	207·78	0·235	0·229
					0·4	207·59	0·190	0·183

* See Eq. (17).

Since $T_i(x)$ is known for the full numerical solutions, values of q/q_{Nu} as calculated from equation (17) can be compared with "exact" values. Typical results of such calculations are given in Table 3, where it may be seen that the predicted values lie within the accuracy claimed for the numerical solutions themselves. Thus, the major source of error in applying equations (17), (18) and (22) is the prediction of the mass transfer conductance.

REFERENCES

1. V. E. DENNY, A. F. MILLS and V. J. JUSIONIS, Laminar film condensation from a steam–air mixture undergoing forced flow down a vertical surface, *J. Heat Transfer* **93**, 297–304 (1971).
2. W. J. MINKOWYCZ and E. M. SPARROW, Condensation heat transfer in the presence of noncondensables, interfacial resistance, superheating, variable properties, and diffusion, *Int. J. Heat Mass Transfer* **9**, 1125–1144 (1966).
3. E. M. SPARROW and S. H. LIN, Condensation heat transfer in the presence of a noncondensable gas, *J. Heat Transfer* **86**, 430–436 (1964).
4. W. J. MINKOWYCZ, Laminar film condensation of water vapor on an isothermal vertical surface, Ph.D. dissertation, University of Minnesota (1965).
5. V. E. DENNY and A. F. MILLS, Nonsimilar solutions for laminar film condensation on a vertical surface, *Int. J. Heat Mass Transfer* **12**, 965–979 (1969).
6. A. F. MILLS and R. A. SEBAN, The condensation coefficient of water, *Int. J. Heat Mass Transfer* **10**, 1815–1827 (1967).
7. S. V. PATANKAR and D. B. SPALDING, A finite difference procedure for solving the equations of the two dimensional boundary layer, *Int. J. Heat Mass Transfer* **10**, 1389–1411 (1967).
8. R. IGLISCH, Exact calculation of laminar boundary layer in longitudinal flow over a flat plate with homogeneous suction, NACA T.M. 1205 (1949).
9. D. B. SPALDING, *Convective Mass Transfer*. McGraw-Hill, New York (1963).
10. A. ACRIVOS, Mass transfer in laminar-boundary-layer flows with finite interfacial velocities, *A.I.Ch.E. Jl* **6**, 410–414 (1960).
11. E. A. MASON and L. MONCHIK, Transport properties of polar gas mixtures, *J. Chem. Phys.* **36**, 2746–2757 (1962).
12. J. HILSENRATH, *Tables of Thermodynamic and Transport Properties of Gases*. Pergamon Press, New York (1960). Also National Bureau of Standards Circular No. 564 (1955).
13. J. H. KEENAN and F. G. KEYES, *Thermodynamic Properties of Steam*, Wiley, New York (1949).
14. J. O. HIRSCHFELDER, C. F. CURTIS and R. B. BIRD, *Molecular Theory of Gases and Liquids*. Wiley, New York (1954).
15. I. W. BUDDENBERG and C. R. WILKE, Viscosities of some mixed gases, *J. Phys. Colloid. Chem.* **55**, 1491–1498 (1951).
16. R. S. BROKAW, Alignment charts for transport properties viscosity, thermal conductivity, and diffusion coefficients for nonpolar gases and gas mixtures at low density, NASA Technical Report R-81 (1960).

17. R. A. SVEHLA, Estimated viscosities and thermal conductivities at high temperatures, NASA-TR R-132 (1962).
18. *Matheson Gas Data Book*, 4th Ed. The Matheson Co., Herst Litho, New York (1966).
19. R. R. DREISBACH. *Physical Properties of Chemical Compounds*–II, Advances in Chemistry Series No. 22. American Chemical Society (1959).
20. *Handbook of Chemistry and Physics*, 44th Ed. The Chemical Rubber Publishing Co., Cleveland (1962).
21. C. D. HODGMAN, *Handbook of Chemistry and Physics*, 42nd Ed. Chemical Rubber Publishing Co. (1961).
22. *Ethyl Alcohol*. Enjay Chemical Publishing Co., New York (1962).
23. *American Institute of Physics Handbook*, 2nd Ed. McGraw-Hill, New York (1963).

INFLUENCE D'UN GAZ NON CONDENSABLE ET D'UN ÉCOULEMENT FORCÉ SUR UNE CONDENSATION EN FILM LAMINAIRE

Résumé—On présente une étude analytique de l'influence d'un gaz non condensable et d'un écoulement forcé sur une condensation en film laminaire. Du fait du caractère non similaire notable du problème de l'écoulement biphasique couplé, les équations principales de conservation dans la phase vapeur sont résolues numériquement par des moyens relevant d'une technique avancée. Les conditions limites interfaciales ont été à chaque étape extraites d'une analyse du film tombant du type Nusselt localement valable. Dans le liquide les propriétés locales variables ont été évaluées à l'aide du concept de température de référence, tandis que celles dans la vapeur ont été calculées selon la théorie cinétique.

On a présenté les résultats du transfert thermique sous la forme q/q_{Nu} en fonction de x pour six vapeurs d'eau, d'ammoniaque, de Fréon 12, d'éthanol, de butanol, et de tétrachlorure de carbone recondensant sur une surface verticale à la température de 25,5°C. On a obtenu des résultats pour des vitesses pour la vapeur de 0,30 et 3 m/s pour des températures de saturation de 32,2, 37,7 et 48,8°C, et pour des concentrations massiques d'air égales à 0,00 let 0,01. Guidé par les résultats numériques, on développe une méthode de calcul semi-empirique qui donne une base satisfaisante pour les calculs "d'engineering".

EINFLUSS VON INERTGAS UND ZWANGSSTRÖMUNG AUF DIE LAMINARE FILMKONDENSATION

Zusammenfassung—In einer analytischen Studie wird der Einfluss eines nichtkondensierbaren Gases und der Zwangsströmung auf die laminare Filmkondensation untersucht. Wegen des ausgeprägten nichtähnlichen Charakters des gekoppelten Zwei-Phasen-Strömungsproblems wurden die bestimmenden Erhaltungsgleichungen in der Dampfphase numerisch gelöst mit Hilfe eines fortschreitenden Verfahrens. Die Randbedingungen an der Trennfläche wurden bei jedem Schritt aus einer örtlich gültigen Nusseltbetrachtung des fallenden Films gewonnen. Die örtlich unterschiedlichen Stoffwerte in der Flüssigkeit wurden mit Hilfe der Methode der Bezugstemperatur ermittelt. Die Stoffwerte des Dampfes wurden berechnet in Übereinstimmung mit der kinetischen Theorie. Die Ergebnisse des Wärmeübergangs bei Kondensation an einer senkrechten Oberfläche von 27°C in der Form q/q_{Nu} in Abhängigkeit von x werden für sechs Dampfarten dargestellt: Wasser, Ammoniak, Frigen 12, Äthanol, Butanol und Tetrachlorkohlenstoff. Die Ergebnisse wurden erzielt für Dampfgeschwindigkeiten von 30,5 und 305 cm/s, Sättigungstemperaturen von 32, 38 und 49°C und Luftanteilen bezogen auf die Masse von 0,001 und 0,01. An Hand der numerischen Daten wird eine halbempirische Berechnungsmethode entwickelt, die eine zufriedenstellende Grundlage für ingenieurmässige Berechnungen darstellt.

ВЛИЯНИЕ ТЕЧЕНИЯ НЕСЖИМАЕМОГО ГАЗА И ВЫНУЖДЕННОГО ТЕЧЕНИЯ НА ЛАМИНА РНУЮ ПЛЕНОЧНУЮ КОНДЕНСАЦИЮ

Аннотация—Представлено аналитическое исследование влияния конденсируемого газа и вынужденного течения на ламинарную пленочную конденсацию. Благодаря нехарактерной задаче сдвоенного двухфазного течения, основные уравнения сохранения в паровой фазе решались численно с помощью метода подгонки. Граничные условия на поверхности раздела фаз на каждом этапе вычитались из локальных значений критерия Нуссельта для падающей пленки. Локально изменяемые свойства в жидкости рассчитывались по исходной температуре, в то время как свойства в паре рассчитывались согласно кинетической теории.

Представлены результаты по переносу тепла для шести видов пара—воды, аммиака, фреона −12, этанола, бутанола и тетрахлорида углерода, конденсирующихся на вертикальной поверхности при 80°F. Результаты получены для скоростей пара в 1,0 и 10,0 фут/сек, при температурах насыщения 90, 100 и 120° и массовой концентрации воздуха 0,001 и 0,01.

При помощи численных данных разработан полуэмпирический метод расчета, представляющий удовлетворительную основу для инженерных расчетов.